

Chapter 4

Signatures of Multipolar Fields on the Polarization Position Angle

4.1 The Rotating Vector Model (RVM)

Information about the magnetic field structure in neutron stars can be obtained from polarization measurements. In fact, among the best arguments in favour of the hollow cone model (refer chapters 1 and 2) is the behaviour of the linear polarization observed across the pulse window. As discussed in chapter 1, the linear polarization is expected to be parallel to the projection of the magnetic field lines in the plane of the sky, given the properties of curvature radiation. As the line of sight traverses the emission cone, the linear polarization is thus observed to execute an S-shaped swing across the pulse. Introduced by Radhakrishnan & Cooke (1969) for the Vela Pulsar (PSR B0833-45), this Rotating Vector Model (RVM) has been fairly successful in modelling the observed swings of the polarization position angle in a large number of pulsars, under the assumption of a pure dipole geometry. However, small but significant departures from the polarization swing predicted by a pure dipole are seen in some cases in high time-resolution observations. In this chapter we examine what kind of departures, if any, from the classical dipole RVM may possibly be due to the presence of higher multipole (we will examine the case of only an additional quadrupole) components.

In the case of dipolar field geometry the position angle Ψ can be related to the angle

between the rotation axis and the magnetic axis (α), the angle between the magnetic axis and the line of sight of the observer (β) and the longitude (ϕ), by the relation

$$\tan(\Psi - \Psi_0) = \frac{\sin(\alpha) \sin(\phi - \phi_0)}{\sin(\alpha + \beta) \cos(\alpha) - \cos(\alpha + \beta) \sin(\alpha) \cos(\phi - \phi_0)} \quad (4.1)$$

where a pulse period is in a longitude range 0° to 360° . ϕ_0 and Ψ_0 are offsets in the pulse center and position angle.

Fitting the above relation to the observed position angle traverse a and β can be obtained. The values of α , β obtained by such a fitting procedure is not always well constrained as the pulse duty cycle is generally small and only allows the measurement of the sweep over a small longitude range. Another independent way to obtain the geometrical parameter α is from the core-width measurements (Rankin 1990, also see chapter 2). The steepest gradient in the position angle traverse curve can be related to α and β by the relation,

$$\left(\frac{d\Psi}{d\phi} \right)_{\phi=\phi_0} = \frac{\sin(\alpha)}{\sin(\beta)} \quad (4.2)$$

Knowing the α values from core-width measurements and from the measurement of the steepest gradient of the position angle traverse, β can be estimated. The total change in Ψ is the largest if the beam is cut centrally which means $\beta = 0$. A shallow position angle swing, on the other hand, indicates that the line-of-sight cuts the outer edge of the beam, i.e. the impact angle is large. It should be noted that the slope of the steepest gradient does not give the sign of β as there is no way to distinguish the sense of rotation of the pulsar. It has been shown by Narayan & Vivekanand (1982), that the sign of β can be inferred from the nature of the traverse near the wings of the profile. For positive β values, which is when the line of sight passes between the magnetic dipole axis and the stellar equator, the curve flattens near the profile wings. For lines of sight passing between the magnetic dipole axis and the rotation axis, defined as negative β values, the curve is monotonic in nature.

There are two important assumptions in the RVM. Firstly it is assumed that the observed emission is directed towards the observer as a 'pencil' beam of emission along every longitude, as any finite beam size can cause depolarization of the radiation. Secondly, it assumes that the observed emission is due to relativistic plasma flowing out

of dipolar field lines. Blaskiewicz et al. (1991), however, introduced a new ingredient in the model where they took the corotation of the plasma with the neutron star into account. Due to the motion of the frame of reference of the plasma and the observer, aberration effects can set in. As a result, the emission beam is bent such that the pulse intensity arrives at earlier times by r_{em}/c , where r_{em} is the emission height measured from the center of the star and due to the beaming towards the observer, the steepest gradient of the polarization angle of the sweep curve arrives at later times by about $3r_{em}/c$. Thus, the lag between the center of pulse and the steepest gradient in the position angle curve is $4r_{em}/c$. This aspect was confirmed by Blaskiewicz et al (1991) on a large set of pulsars.

4.2 Multipolar fields and RVM

The presence of multipolar magnetic field components in the emitting region can cause position angle traverse which can be very different from that given by equation(4.1). Of course, this is only true if the emission originates from regions where the magnetic field is significantly non-dipolar. The multipolar components arising at the stellar surface would fall off rapidly compared to the dipole. Thus most of the emission may arise from regions where the magnetic field has acquired a dipolar structure. Pulse width evolution with frequency and position angle traverse for a large body of pulsars seems to support the dipolar picture well. Frequency evolution of pulse widths suggests a "radius-to-frequency" mapping (refer chapters 1 and 2), which essentially says that emission at different frequencies arise from different heights from the surface of the star and higher the frequency the closer is the emission region to the stellar surface. Thus, by observing at different frequencies one is probing different heights from the stellar surface.

It is possible that the picture of a simple dipolar geometry of the magnetic field throughout the emitting region is not true. As one probes regions closer to the star the field structure would have distortions due to multipoles, the most prominent of which would be the quadrupole. Here we simulate the multipolar magnetic field around the

neutron star to illustrate the possible variations in the polarization position angle. We assume that the surface magnetic field is a mixture of a star centered dipole (\vec{B}_d) and a quadrupole (\vec{B}_q). We apply the following procedure in our simulation,

a) We choose a cartesian co-ordinate system (S), where the rotation axis of the neutron star is along the z axis and the origin corresponds to the center of the star. An arbitrary point in S is defined by the co-ordinates (x, y, z) .

b) With respect to S, the magnetic dipole axis is inclined at an angle α , in the yz plane. We choose another co-ordinate system S' , with the dipole axis along the z' axis. The co-ordinates (x, y, z) in S are thus transformed in S' as (x', y', z') by a rotation matrix R as,

$$(x', y', z') = R (x, y, z)$$

The dipolar magnetic field in S' can thus be written as,

$$\begin{aligned} B_{dx'} &= \frac{1.5 x' z'}{r^5} \\ B_{dy'} &= \frac{1.5 y' z'}{r^5} \\ B_{dz'} &= 0.5 \left(\frac{3 z'^2}{r^5} - \frac{1}{r^5} \right) \end{aligned} \quad (4.3)$$

where $(B_{dx'}, B_{dy'}, B_{dz'})$ are the components of the dipolar magnetic field in units of the surface fields and $r = \sqrt{x^2 + y^2 + z^2}$ is the emission height in units of the stellar radius. x, y, z are in units of the stellar radius.

c) We choose another frame S'' which is obtained by rotating through the Euler angles θ_1, θ_2 and θ_3 with respect to the S' frame such that (x', y', z') transforms to (x'', y'', z'') as,

$$(x'', y'', z'') = T (x', y', z')$$

where T is Euler transformation matrix (cf. Goldstein 1980, 'Classical Mechanics', Chapter 4). Further, we choose the magnetic quadrupole moment to be along the z'' axis. The quadrupolar magnetic field in S'' in terms of the spherical co-ordinates (r, θ'', ϕ'') is given by,

$$B_{qr} = \frac{Q}{2} \left(\frac{3 \cos^2 \theta'' - 1}{r^4} \right) \quad (4.4)$$

$$\begin{aligned}
B_{q\theta''} &= Q \left(\frac{\cos\theta'' \sin\theta''}{r^4} \right) \\
B_{q\phi''} &= 0
\end{aligned}$$

where $(B_{\theta}, B_{q\theta''}, B_{q\phi''})$ are the components, in spherical co-ordinates, of the quadrupolar magnetic field which, in cartesian co-ordinates, has components as $(B_{qx''}, B_{qy''}, B_{qz''})$. The fields are in units of the surface field. Q is the ratio of the quadrupole field strength to the dipole field strength at their respective poles at the surface. To obtain the quadrupolar field components in the S^t frame an inverse Euler transformation is applied such that,

$$(B_{qx'}, B_{qy'}, B_{qz'}) = \bar{T} (B_{qx''}, B_{qy''}, B_{qz''})$$

where \bar{T} is the inverse euler transformation matrix and $T\bar{T} = \mathbf{I}$. The resulting magnetic field (\vec{B}') in the S^t frame due to a dipole and quadrupole is computed as, $\vec{B}' = \vec{B}_d' + \vec{B}_q'$, which can be transformed to the S frame as, $\vec{B} = \bar{R} \vec{B}'$. Here \bar{R} is the rotation matrix for transforming the vectors in the S^t to the S frame, such that $\bar{R}\bar{R} = \mathbf{I}$.

d) To find the position angle Ψ , \vec{B} and the spin axis are projected on the plane of the sky separately. Ψ is the angle between these projections. The magnetic field direction is given by the unit vector \vec{b} and let the line of sight be defined by the unit vector \vec{l} . The direction of the projection of the spin axis is given by the unit vector $-\vec{\zeta}$, where ζ is the angle between the rotation axis and the line of sight. Thus the position angle Ψ is computed as,

$$\Psi = -\cos^{-1} \left(\frac{(\vec{b} - (\vec{b} \cdot \vec{l}) \cdot \vec{l}) \cdot \vec{\zeta}}{|\vec{b} - (\vec{b} \cdot \vec{l}) \cdot \vec{l}|} \right) \quad (4.5)$$

Assuming that the linear polarization is along the projected magnetic field lines, the position angle curve would deviate from that expected from a dipole geometry. The quadrupole field would die off faster as a function of distance from the stellar surface. Since the emission at lower frequencies originate further away from the stellar surface, the position angle curve for these frequencies would more closely represent the dipole-field geometry than that at higher frequencies. This effect can be studied by establishing the position angle sweep curves for a wide range of frequencies for a

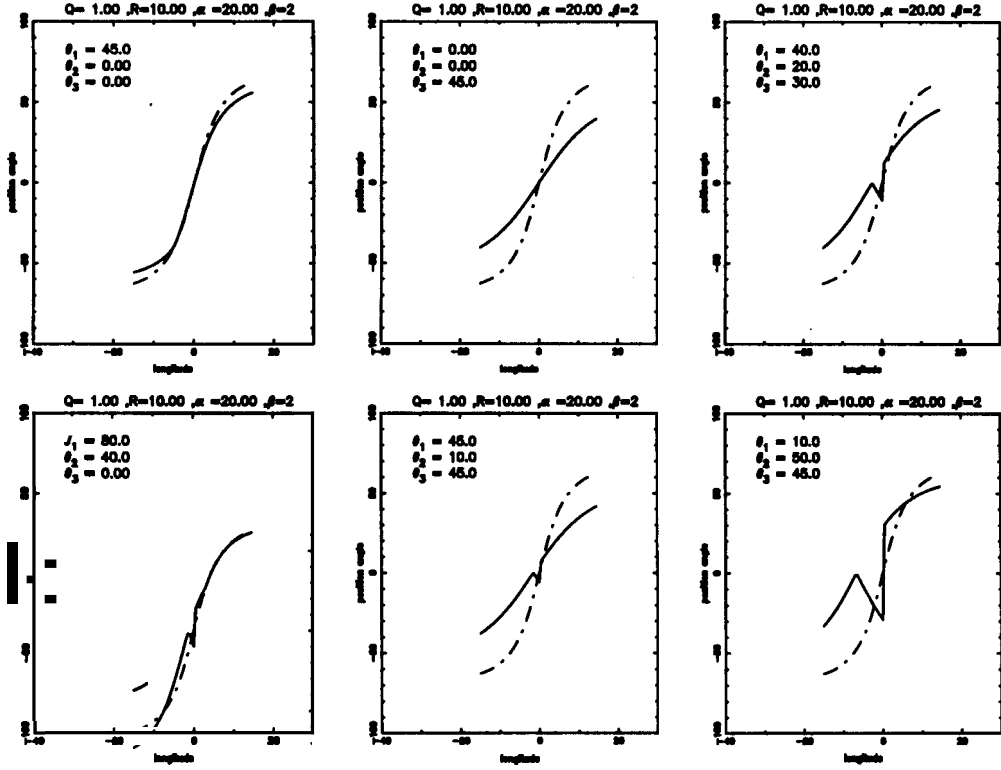


Figure 4.1: Simulations illustrating the polarization position angle sweep curves due to a mixture of dipole and quadrupole magnetic field. The dash-dot line in the above plots shows the position angle traverse for $\alpha = 20^\circ$ and $\beta = 2^\circ$. The continuous line shows the position angle traverse for various orientations of the dipole with respect to the quadrupole, as specified by the euler angles θ_1 , θ_2 and θ_3 in each plot. The constant $Q = 1$ in all the six cases shown above the emission height is 10 times the stellar radius.

given pulsar. The procedure would be to use the position angle curve at a sufficiently low frequency to obtain the values of α and β by fitting equation (4.1), and to fit the position angle curve using these values of α and β at higher frequencies. Any significant deviation would reflect the presence of multipole fields.

Figure (4.1) shows the simulated polarization position angle curves obtained for a pure dipole field (dashed lines in the figure) in comparison to those for a mixture of dipole and quadrupole fields (continuous lines in the figure) for various combinations of θ_1 , θ_2 and θ_3 . The curves are simulated for $\alpha = 20^\circ$, $\beta = 2^\circ$, $Q = 1$ and $r = 10$. In figure (4.2), we show the variation of the position angle curves for $\theta_1 = 40^\circ$, $\theta_2 = 20^\circ$ and $\theta_3 = 5^\circ$ for various values of Q and r as indicated in the figure. There are important

trends that should be noticed in the figures. The sudden jumps in the polarization position angle near the center of the profile for certain orientations can have observable effects. The span of the position angle curve changes in such a way that the resulting curve could be interpreted to be a traverse corresponding to a different effective β . In principle, one could then extract the complete magnetic structure of the pulsar by a detailed analysis of the polarization position angle curves. However, as is evident from the above discussion, the number of unknowns that one has to solve for in order to fit a non-dipolar position angle traverse are enormous. In the case of a quadrupole the unknowns are the relative orientation of the quadrupole with respect to the dipole and the strength of the quadrupole, in addition to the usual α and β . Making such a detailed fit to extract all the parameters of the multipole structure would not be meaningful for most of the existing observations. Thus the purpose of the exercise here is only to establish the overall trends in the position angle traverse which could be associated with an underlying non-dipolar magnetic field.

To probe the existence of non-dipolar fields it would be necessary to observe a pulsar over a wide range of frequencies, from as low as 100 MHz to as high as **33** GHz. The pulsar chosen should be strong enough to be seen over this entire frequency range. It is important to do a single pulse analysis to resolve the PA curve. The reason for this is that pulsars are well known to show orthogonal position angle flips (refer chapter 1). An average profile without separating the polarization modes would therefore not be able to establish the polarization position angle curve correctly. It is also important to choose a pulsar with high degree of linear polarization.

We have carried out this investigation in detail for the pulsar PSR,B0329+54 which is discussed in the rest of the chapter. The possible dependence of the position angle curve on frequency may arise due to the following reasons:

- 1) Relativistic aberration effects in the pulsar magnetosphere, will cause a displacement in the position angle curve with respect to the profile center. This will only cause a shift of the RVM preserving the values of a and β at all frequencies (Blaskiewicz et al. 1991).

- 2) If non-dipolar components of the magnetic field are present, then the position

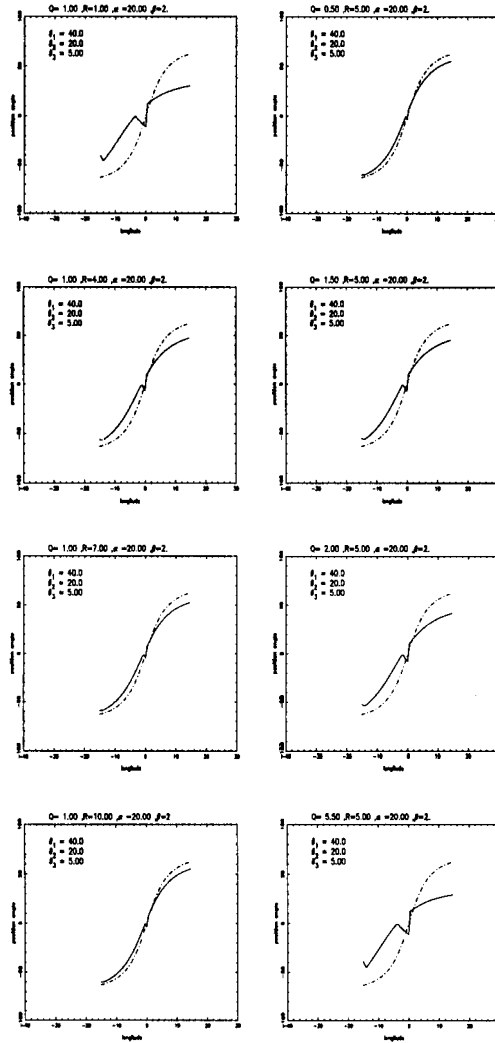


Figure 4.2: Simulations of the polarization position angle for a mixture of dipole and quadrupole magnetic field as a function of increasing emission height (left hand panels) and increasing values of the parameter Q (right hand panels). The dashed line in each panel corresponds to the RVM for $\alpha = 20''$ and $\beta = 2''$. The continuous curves in each panel are the simulated curves. For all the illustrated curves $\alpha = 20''$ and $\beta = 20^\circ$. In the left, hand panels $Q=1$ for all the 4 cases, while the emission height is 1, 4, 7, and 10 times the stellar radius respectively from top to bottom. In the right hand panels the emission height is held constant as 5 times the stellar radius, while $Q=0.5, 1.5, 2$ and 5.5 respectively from top to bottom.

angle traverse can develop kinks at higher frequencies. These kinks may, however, not be observable unless the time resolution employed is very high. Instead, the dipolar RVM fit through the data would yield values of β (cf. equation 4.1 and 4.2) that are frequency dependent.

4.3 Multifrequency Polarization Characteristics of PSR B0329+54

4.3.1 PSR B0329+54

This is one of the brightest pulsars known and has been studied in great detail over a wide range of radio frequencies. Based on the phenomenological study of pulsar classification, Rankin (1993) (also see chapters 1 and 2), classifies this pulsar as a Triple or a possible Multiple. Although the integrated pulse profile shows three clearly identifiable components (see Fig. 4.3), Kramer (1994) based on a gaussian fitting procedure established the presence of five components over a wide range of frequencies. More recently Gangadhara & Lorimer (1999) have reported the existence of at least nine components in this pulsar. This pulsar is also known to exhibit mode changing (refer chapter 1) at any frequency and the profile appears to switch between three to five components depending on the mode (Bartel et al 1982, Xilouris et al, 1995). The components of the less often occurring (abnormal) mode at low frequencies are slightly displaced with respect to the more often occurring (normal) mode (McKinnon & Hankins, 1992, Xilouris et al, 1995). The leading part of the profile is highly polarized during both the modes at 1.7 GHz (Bartel et al, 1982). However at 10.55 GHz this part of the profile is completely depolarized (Xilouris et al, 1995). The central part of the profile is moderately polarized at low frequencies and *jumps* in the position angle curves are prominent. At 10.55 GHz the central part shows complete depolarization. In the trailing part of the profile the position angles for two modes differ, although not substantially (Bartel et al, 1982). The average position angle sweep curve for this pulsar is extremely complicated and does not fit well with the RVM. However, it was demonstrated by Gil & Lyne

(1995) that a single pulse study at 408 MHz reveals the presence of two orthogonal position angle modes for this pulsar, each of which is individually in agreement with the RVM.

Here we are interested in comparing the position angle sweep curves at different frequencies as already discussed in section (4.1). If the emission originates from regions where the magnetic field has a dipolar structure we do not expect any change in the shape of the position angle sweep curve which can be explained using the RVM. However, any significant change in the curve would call for an alternative explanation. We investigate this for PSR 0329+54 at 1.412 , 2.695 and 4.850 GHz. We also compare our results with the position angle sweep curve at 408 MHz published by Gil & Lyne (1995). We have used a sequence of single pulse data stream for PSR B0329+54 at these frequencies from the European Pulsar Network (EPN) archives supplied to us by Alexis Von Hoensbroech and R. Wielebinski (Max-Planck Institut for Radioastronomie, Bonn).

4.3.2 Data Analysis

The pulse data sequence at each frequency is available in the form of four stokes parameter $I(i, j), Q(i, j), U(i, j)$ and $V(i, j)$, where $i = 1, \dots, N_{\text{pul}}$ refers to the pulse number out of N_{pul} pulses and $j = 1, \dots, N_{\text{bin}}$ refers to the j^{th} bin in the profile out of N_{bin} points. The position angle for each sample were calculated according to $\Psi(i, j) = \frac{1}{2} \tan^{-1}[U(i, j)/Q(i, j)]$. The linear polarization $L(i, j) = \sqrt{Q(i, j)^2 + U(i, j)^2}$, were calculated for each sample. The average total intensity (I_{ave}), linear polarization (L_{ave}), circular polarization (V_{ave}) and position angle (Ψ_{ave}) for j^{th} bin in the pulse profile were calculated as,

$$I_{\text{ave}}(j) = \sum_{i=1}^{N_{\text{pul}}} I(i, j)/N_{\text{pul}}, \quad (4.6)$$

$$L_{\text{ave}}(j) = \sqrt{\left(\sum_{i=1}^{N_{\text{pul}}} Q(i, j)/N_{\text{pul}}\right)^2 + \left(\sum_{i=1}^{N_{\text{pul}}} U(i, j)/N_{\text{pul}}\right)^2}$$

$$V_{\text{ave}}(j) = \sum_{i=1}^{N_{\text{pul}}} V(i, j)/N_{\text{pul}}$$

$$\Psi_{\text{ave}}(j) = \frac{1}{2} \tan^{-1} \left[\frac{\sum_{i=1}^{N_{\text{pul}}} U(i, j)}{\sum_{i=1}^{N_{\text{pul}}} Q(i, j)} \right]$$

respectively. The average total intensity, linear polarization, circular polarization and the position angle for 1.4, 2.695 and 4.85 GHz are shown in figure (4.3). As already mentioned we are interested in comparing the position angle sweep curves over this wide range of frequencies. Since pulsars are well known to exhibit two polarization modes, the average position angle curve can be of extremely complicated nature. A single pulse analysis is absolutely essential to separate the two polarization modes. One of the standard ways of separating the modes is to produce a distribution of the frequency of occurrence of single pulse position angle at every longitude (Gil & Lyne, 1995). At any given longitude the peak of the distribution would indicate the mean position angle for the preferred mode. If the distribution is bimodal, exhibiting two peaks, then this indicates the existence of two modes, which can then be separated using this distribution. In general, the two modes are separated by about 90° (orthogonal modes). The polarization position angle itself, as obtained from equation (4.7), is defined modulo 180°. If the linearly polarized power is low, however, the position angles determined from a noisy data can lead to spurious results which can affect the resulting distribution of position angles. In our analysis we consider only the samples for which $L(i, j)^2 > \sigma_u(i)^2 + \sigma_q(i)^2$ (Gil et al, 1991), where $\sigma_u(i)$ and $\sigma_q(i)$ are the standard deviations for the stokes parameter Q and U for the i^{th} pulse calculated in the off pulse region. For good polarization measurements $\sigma_u(i)$ and $\sigma_q(i)$ should be of the same order and thus the above criteria simply implies that samples for which $L(i, j) > \sqrt{2}\sigma_{u,q}$ are used. The error in the position angle is calculated using,

$$\sigma_{\Psi} = \frac{1}{2L(i, j)^2} \sqrt{(Q(i, j)\sigma_q(i))^2 + (U(i, j)\sigma_u(i))^2} \quad (4.7)$$

The above expression is obtained by the propagation of error in calculating Ψ , where errors in U and Q are uncorrelated. Figures (4.5, 4.7, 4.8) shows the grey-scale representation of the frequency of occurrence of position angles as a function of pulse longitudes for 1.4, 2.695 and 4.850 GHz respectively. The whole range of position angle is plotted twice for clarity.

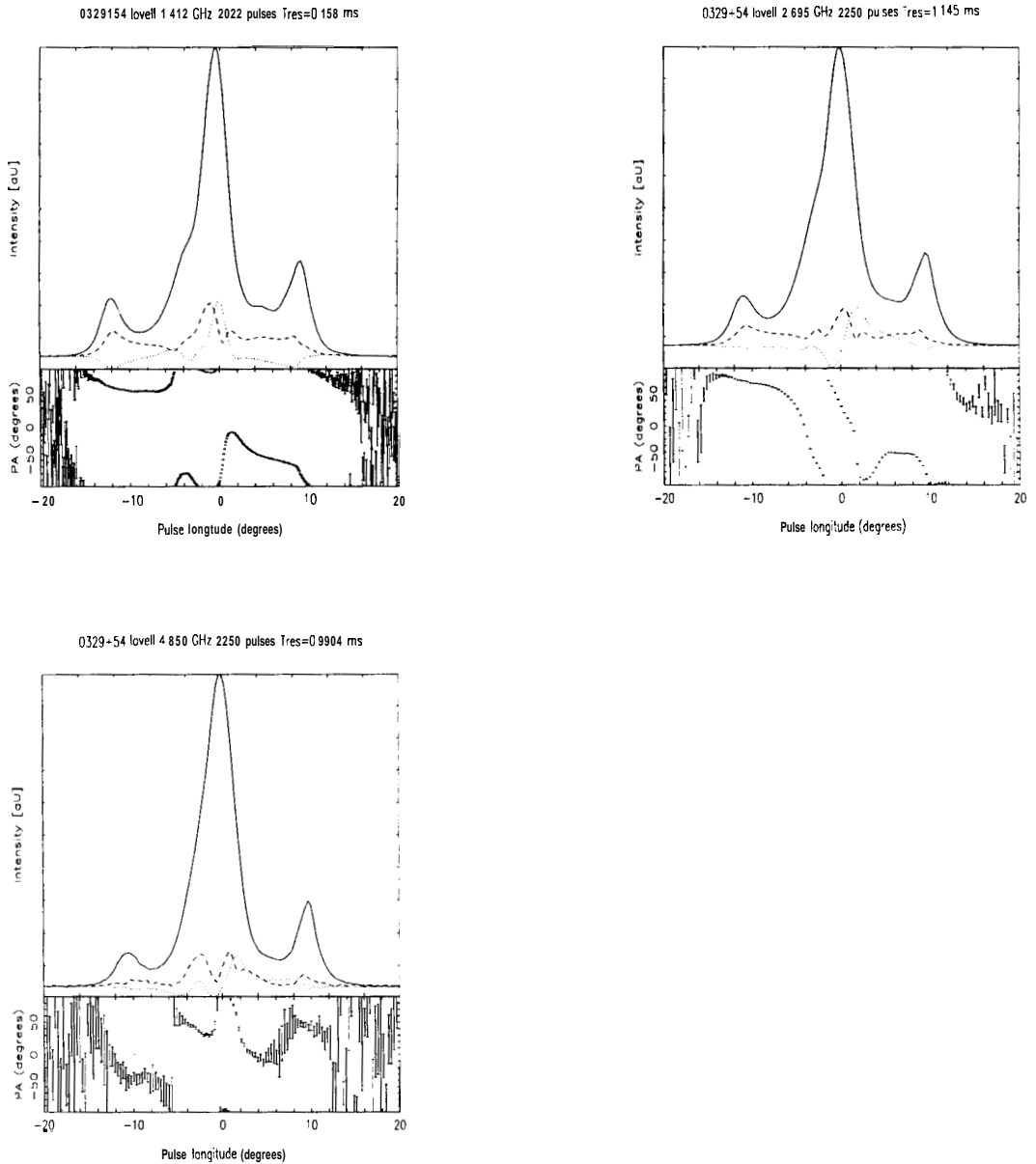


Figure 4.3: Full polarization average profiles of PSR B0329+54 at 1.412, 2.695 and 4.850 GHz. In the top panel of each plot the continuous curve is the total intensity I , the clashed curve is the linear polarization L and the dotted curve is the circular polarization V as obtained using equation 4.7. The bottom panel in each plot the average position angle, as given by equation 4.7 is plotted, with the error bars calculated using equation 4.7.

4.3.3 Polarization modes at 0.408 GHz

The polarization position angle modes in this pulsar at 0.408 GHz has been extensively studied by Gil & Lyne (1995). They find that the polarization modes follow two parallel tracks each consistent with the RVM and they are separated by about 90° . At the leading edge of the profile there is a rapid orthogonal jump at longitude -13° from the secondary mode to the primary mode which begins to dominate (refer Fig 4.4). In the leading part of the profile between -13° to -10° the primary mode dominates which goes through a slow orthogonal transition at $-7''$ longitude where the secondary mode takes over. The secondary mode dominates between longitudes $-4''$ to $-2''$ under the small component at that longitude. The position angle then returns to the primary mode between longitudes -1° to 2° and dominates up to $5''$. At the trailing edge of the profile between longitudes $9''$ to $15''$ both the modes seems to be present with the secondary mode dominating over the primary one. The mean position angle sweep curve is shown as a solid line and its complexity is evident. It is also clear from the figure that the mode separated curves individually fit the RVM well and the fitted curves are shown for the primary (squares) and secondary (circles) modes respectively.

Gil & Lyne (1995) have fitted the RVM given by equation (4.1) to the the separated modes and found the best fit values for α, β, ϕ_0 and Ψ_0 for the two modes separately. For the primary mode they find $\alpha = 42'' \pm 20^\circ$, $\beta = -3'' \pm 2^\circ$, $\phi_0 = 2'' \pm 1^\circ$ and $\Psi_0 = 184^\circ \pm 3''$ and for the secondary mode, $\alpha = 59^\circ \pm 20''$, $\beta = -4.5^\circ \pm 1.5''$, $\phi_0 = 2^\circ \pm 1''$ and $\Psi_0 = 94'' \pm 3^\circ$ respectively. It is important to note that such a fitting procedure is not able to unambiguously determine the sign of β . Thus the fitting procedure gives the mean α and β to be 51° and $4''$. The conclusion drawn by Gil & Lyne (1995) from this exercise is that the polarization mode at 0.408 GHz for this pulsar follows the S-shaped RVM which means that the emission necessarily arises from a dipolar magnetic field geometry as predicted by the model. Also, if the radiation motles are strictly orthogonal, the position angle should follow either one mode or the other. It has been noted by Gil & Lyne (1995) that significant amount of non-orthogonal radiation is observed near the pulse center. This is attributed to the possible finite beam width of the radiation process, which might result in radiation from nearby field lines being

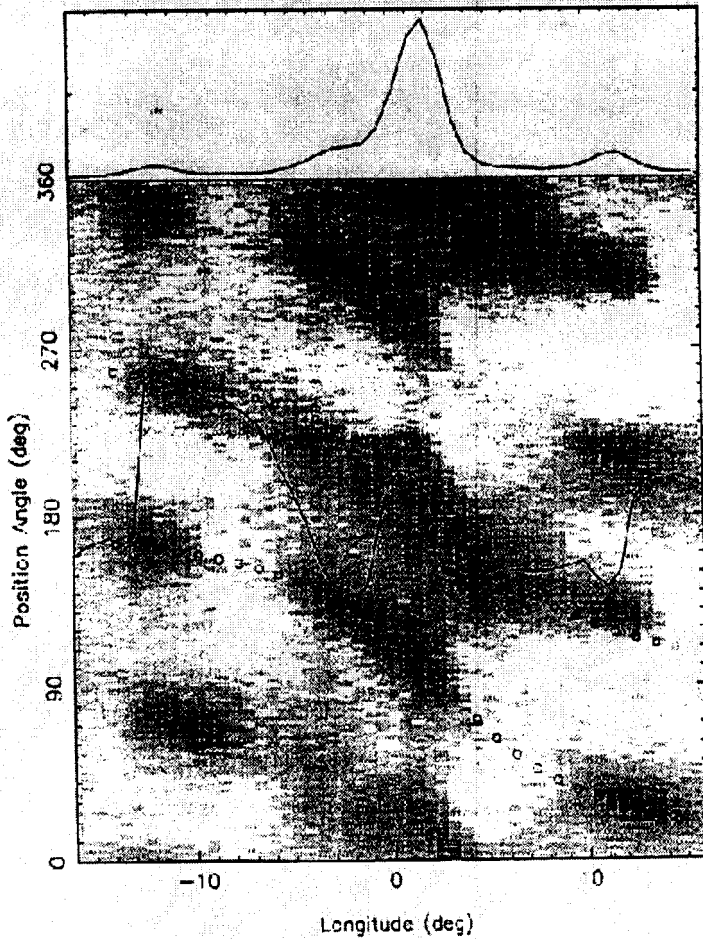


Figure 4.4: The above figure is adopted from Gil & Lyne (1995). Grey scale representation of the frequency of occurrence of the polarization position angle as a function of longitude for 2000 pulses at 408 MHz. The whole range of position angle is plotted twice for clarity. The average position angle is shown by the continuous curve. The RVM for the primary mode (squares) and secondary mode (circles) are fitted to the data. The RVM for the two modes are same but only separated by $90''$ and has $\alpha = 51^\circ$, $\beta = 2^\circ$ and $\phi_0 = 2^\circ$.

directed along the line of sight. This effect is rather prominent near the pulse center which corresponds to the center of the dipole magnetic field where the field lines are divergent in nature. From the RVM $(d\Psi/d\phi)_{\phi=\phi_0} = \sin(\alpha)/\sin(\beta)$ and for $\alpha = 51''$ and $\beta = -4^\circ$ it is $-11.4^\circ/''$ which is in good agreement with the value measured from the steepest gradient observed in the position angle curve which is measured to be $-11^\circ/''$.

Another interesting point to note is the non-orthogonal radiation observed between the longitude range 10° to 14° . Clearly the fitted RVM for the primary mode (square) does not fit the high frequency of occurrence well. The separation between these non-orthogonal modes are $\sim 105^\circ$. It is also to be noted that the ratio of the trailing component height to the leading component height is greater than 1, thus indicating that the pulsar was probably observed during the normal mode.

4.3.4 Polarization modes at 1.412 GHz

We have used a sequence of 2022 single pulses at 1.412 GHz to obtain the position angle variations across the pulse profile. The data was obtained using the 76-m Lovell radio telescope at Jodrell Bank during the simultaneous observing experiment with the Effelsberg 100-m telescope as a part of the EPN campaign. The grey-scale representation of the frequency of occurrence of the position angle is shown in figure (4.5) and the average position angle is shown in figure (4.3). Note that the zero longitude of the pulse is chosen arbitrarily and does not correspond to the center of the pulse. The leading component is dominated by the primary mode which is strong between -13° to -7° . Between longitudes $-7''$ to $-4''$ the position angle slowly goes to the secondary mode and then dominates up to -1° . There is a sharp transition observed from the secondary mode to the primary mode between 0° to $-1.5''$ longitude. The primary mode is dominant at most of the trailing part of the profile between $2''$ to $8''$. Between $8''$ to $10''$ the position angle goes sharply to the secondary mode, but only rotates by 70° .

Single pulse mode separated position angle variation of this pulsar at 1.75 GHz has been investigated by Bartel et al (1982). The position angle variation in the leading part of the profile at 1.75 GHz is in good agreement with our results at 1.412

0329+54 lovell 1.412 GHz 2022 pulses Tres=0.158 rns

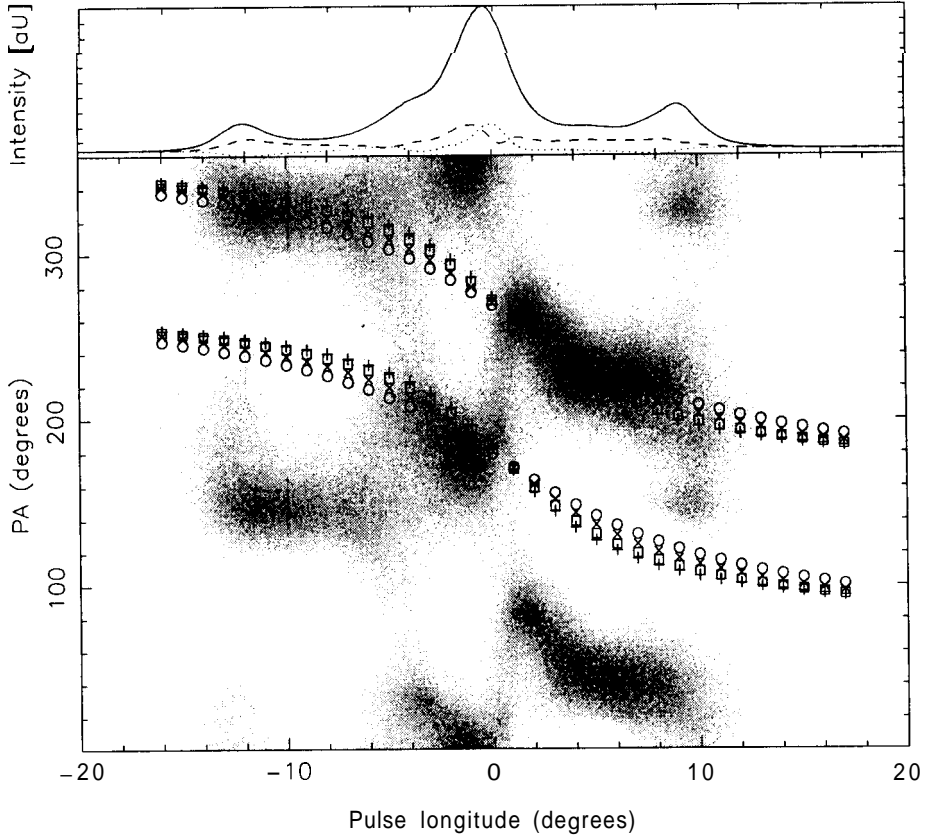


Figure 4.5: The bottom panel in the figure is the grey scale representation of the frequency of occurrence of the polarization position angle at 1.412 GHz. The dark regions corresponds to high frequency of occurrences. The position angle is plotted twice for clarity. The RVM is plotted for the primary mode (the upper curves) and the secondary mode (lower curves) where the upper curve is only fitted. The RVM is displayed for four different α values: namely 30° (circles), 40° (crosses), 50° (squares) and 60° (plus) for fixed $\beta = -3.49^\circ$, $\Psi_o = 263.7^\circ$ and $\phi_o = 0.74^\circ$ respectively. Note that for such widely varving α values used the curves are hardly distinguishable (see section 4.3.4 for discussion). The lower curves are plotted by shifting the upper curves by 90° . The best fit parameters for the RVM of the primary mode (upper curves) are $\alpha = 32.5^\circ$, $\beta = -3.49^\circ$, $\Psi_o = 263.7^\circ$ and $\phi_o = 0.74^\circ$ The upper panel shows the average quantities: intensity (continuous line), linear polarization (dashed line) and circular polarization (dotted line).

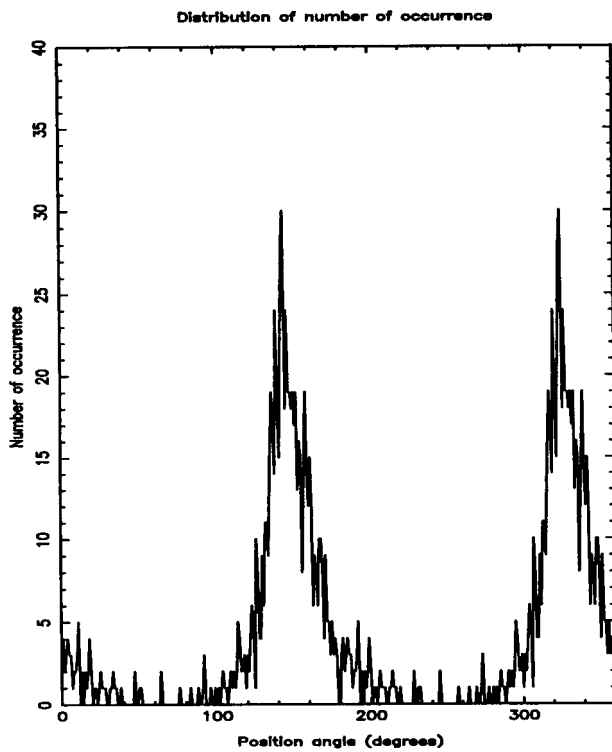


Figure 4.6: The above plot shows the distribution of the number of occurrences as a function of the polarization position angle at longitude -9° for PSR B0329+54 at 1.412 GHz. The polarization position angle is plotted twice for clarity. See section (4.3.4) for details.

GHz. However at the center of the profile the position angle distribution dominates at the primary mode (between -1° to $+1^\circ$ in their plots) while a dominance of the secondary mode is observed in our case. At the trailing edge of the profile there is a non orthogonal transition of about 105° from the primary to the secondary mode at 1.75 GHz, compared to the 70° seen in 1.412 GHz. We divided our data set into four segments into each containing ~ 500 pulses and the integrated profiles on each case had the trailing component dominating over the leading one, and thus we conclude that the pulsar is in the normal mode.

Apart from the above mentioned complications the underlying position angle curve is in good agreement with the RVM. We have fitted the RVM given by equation (4.1) to the primary mode alone as the absence of the secondary mode in most of the profile would make it extremely difficult to constrain the fitted curve using the secondary mode. In order to fit the curve we have used the distribution of the frequency of occurrence of position angles to identify a particular mode. For a given longitude the distribution peaks at a particular position angle. Figure (4.6) shows the distribution of the frequency of occurrence at longitude -9° . It is clear that the distribution peaks at one particular value of the position angle and has a spread around this value. For a given mode we fit a gaussian to this distribution and choose the $1/e$ points on either side of the mean to obtain the range of position angles which we attribute to that given mode. This is done for every longitude where we find a strong signature of the mode. We then use the position angles in the range as identified above for all relevant longitudes to fit equation (4.1). The errors in each sample are given by equation (4.7). There are four free parameters which have to be fitted for, namely α , β , ϕ_0 and Ψ_0 . It is important to note that while fitting such a distribution of points it is extremely difficult to constrain α as various combinations of α and β can give a fit which would have a very similar traverse characteristic. This is also apparent from the similar values of the reduced χ^2 defined as,

$$\chi^2 = \frac{1}{N} \sum_{i=1}^N \left(\frac{\Psi_m(j) - \Psi(j)}{\sigma_\Psi(j)} \right)^2 \quad (4.8)$$

where N is the number of data points to be fitted, $\Psi_m(j)$ is the position angle at a given

longitude j given by the model and $\Psi(j)$ is the observed value. In figure (4.5) there are four curves corresponding to widely different a values ranging between $60''$ to 30° for approximately same β values keeping Φ_\circ and Ψ_\circ constant. The χ^2 obtained for each case is ~ 7.5 , and the model curves can hardly be distinguished. The allowed range for a is 0° to $90''$ and such a large variation cannot constrain a meaningfully. It is thus important to get an estimate of a from other considerations. As mentioned in chapters 1 and 2, a reliable estimate of a comes from the core-width measurements which for this pulsar yield $a = 32.5''$. We adopt this value of a in our fitting procedure as a fixed value and solve for β , ϕ_\circ and Ψ_\circ . We have used the Levenberg-Marquardt method for a nonlinear least-squares fit to the data of the model given by equation (4.1). This method is rather sensitive to the supplied initial guesses for the parameters and thus various sets of initial guesses were used to converge to solutions¹ corresponding to the minimum χ^2 . The best fit values obtained are $\beta = -3.49^\circ \pm 2^\circ$, $\Psi_\circ = 263.7'' \pm 20''$ and $\phi_\circ = 0.74'' \pm 1^\circ$ with $\chi^2 = 7$. The error in the a value, obtained by fixing the other parameters to their mean values is $\pm 10^\circ$. The steepest gradient in the curve $(d\Psi/d\phi)_{\phi=\phi_\circ}$ as measured from the secondary mode lying between longitude $-4''$ and 0° is about $-10 \pm 3^\circ/^\circ$ which is consistent with $\sin(\alpha)/\sin(\beta) = -8.8^\circ/^\circ$ as obtained from the best fit values.

From the above fitting procedure we conclude that the position angle curve of the primary mode is in good agreement with the RVM. The a and β values obtained is consistent, within the given error bars, with the values obtained at 0.408 GHz. Following RVM, it can be said that the emission at 0.408 GHz and up to 1.412 GHz arises from regions having dipolar magnetic field structure.

4.3.5 Polarization modes at 2.695 GHz

A sequence of 2264 pulses observed during various observing programs using the Effelsberg 100-m radio telescope were used to produce the grey-scale representation of the frequency of occurrence of the position angles as shown in figure (4.7). The average

¹We have used the MPFITFUN function available in the Interacting Data Language (IDL) package for our fitting purpose.

0329+54 effberg 2.695 GHz 2250 pulses $T_{res}=1.145$ ms

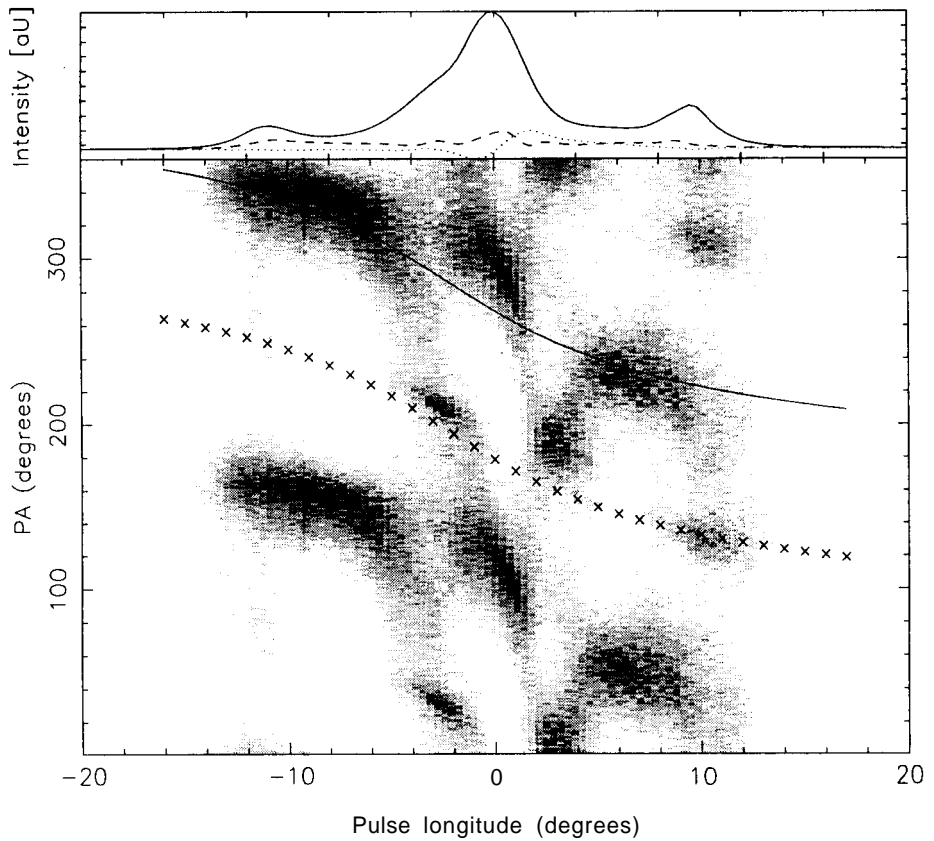


Figure 4.7: The bottom panel of the above plot shows the grey scale representation of the position angles at 2.7 GHz. The RVM is plotted for the primary mode (continuous line) with $\alpha = 32.5^\circ$, $\beta = -3^\circ$, $\Psi_o = 290^\circ$ and $\phi_o = -2.7''$ respectively (see section 4.3.5 for discussion). The secondary mode (with crosses) is the same as the primary mode but shifted by 90° . The upper panel shows the average quantities: intensity (continuous line), linear polarization (dashed line) and circular polarization (dotted line).

position angle sweep curve is shown in figure (4.3). For the leading part of the profile between -11° to $-6''$ longitude the polarization is dominant in the primary mode. Following a slow rotation between $-6''$ to -4° longitude the polarization mode switches to the secondary and continues to remain in that mode up to about $-2''$ longitude. A sharp non-orthogonal transition to the primary mode happens at about $-2''$ and the primary mode dominates up to about $0.5''$. A non-orthogonal jump relatively slowly to the secondary mode is noticed at $2''$ which is dominant up to about $4''$ and then rotates back to the primary mode. The primary mode is dominant between $5.5''$ to $9''$ longitude. Below the trailing component of the profile beyond 10° longitude there is a faint signature of the secondary mode dominating up to 12° . The trailing component height is higher than the leading component height indicating the pulsar is observed in the normal mode.

The position angle traverse characteristic is extremely complicated at this frequency. The S-shaped RVM does not seem to hold true across the pulse profile. If the emission at all frequencies arises from regions where the magnetic field structure is dipolar in nature then the angles α and β , which defines the position angle traverse, should be same at all frequencies. We have already seen that the traverse characteristics for this pulsar at 408 MHz and 1.412 GHz is very similar in nature, both consistent with $\alpha \sim 32.5^\circ$ and $\beta \sim -3.5''$. Adopting the same values, we have fitted the RVM to the primary mode as identified above. The fitting procedure is explained in section (4.3.4). The χ^2 obtained for the fit is ~ 16 which is relatively a bad fit compared to the 1.412 GHz where $\chi^2 \sim 7$. Treating β as a free parameter, the fits were repeated and the best fit values obtained were $\beta = -2.8'' \pm 1.5^\circ$, $\Psi_0 = 266.2'' \pm 15''$ and $\phi_0 = 2.42'' \pm 1^\circ$ with $\chi^2 \sim 15$. Following such high value of χ^2 it is evident that RVM does not fit well to this position angle traverse. The kinky feature lying between longitude $\sim 0^\circ$ to 1° in the primary mode corresponds to the steepest gradient in the curve which gives $(d\Psi/d\phi)_{\phi=\phi_0} = \sin(\alpha)/\sin(\beta) \sim -50^\circ/^\circ \pm 5^\circ$, which for $\alpha = 32.5^\circ$ gives $\beta = -0.6^\circ$. Such a value of β , however, gives an extremely bad fit to most of the position angle traverse. Rejecting the kinky portion a fit was done to the rest of the position angle curve keeping α fixed at, $32.5''$. The best fit values for this case is $\beta = -3'' \pm 1^\circ$,

$\Psi_0 = 290^\circ \pm 15''$ and $\phi_0 = -2.7'' \pm 1^\circ$. The position angle traverse corresponding to these values are plotted in figure(4.7), where the continuous line corresponds to the primary mode and the crosses correspond to the orthogonal mode. The steepest gradient part in the secondary mode lying between longitude $\sim -4''$ to $-2''$ is measured to be around $-10^\circ/^\circ$, which is also consistent, with that observed at lower frequencies. However, between $2''$ to $4''$ longitude a considerable amount of non-orthogonal moding is observed in between the two modes, closer (about $30''$ away) to the secondary mode. Apart from this structure the rest of the secondary mode is in good agreement with the RVM.

From the above exercise we have clearly demonstrated that the position angle traverse at 2.695 GHz is quantitatively different from that at 408 MHz and 1.412 GHz. Two highly intense features between longitudes -1° to 4° (refer Fig.4.7), one of which has a steep gradient and is about $30''$ away from the primary mode and the other about $30''$ away from the secondary mode are present at 2.695 GHz, while no such features are evident at lower frequencies (down to 408 MHz). We have also established that, apart from these kinky features the rest of the position angle curve seems to obey the RVM quite well.

The presence of the two nearly orthogonal modes at the position angle traverse seems to be related to the hollow cones of emission. This characteristic is clearly visible for this pulsar in this frequency, but not so clearly at the lower frequencies, though there are obvious signatures. In figure (4.7) the leading part of the profile between longitudes -14° to $-6''$ defines approximately the existence of the outer conal component. Corresponding to the rising edge of this component between $\sim -14^\circ$ to -11° the two polarization modes are seen to be present at a very low level. There is a significant amount of mode mixing and depolarization at the rising edge of the profile. For the rest of the component there is absolute domination of the primary mode up to $\sim -6''$ longitude. At the trailing end of the profile, between longitude $\sim 5^\circ$ to 14° , the trailing component shows a very similar polarization behaviour to the leading component. The inner part of the component between $\sim 5''$ to 9° longitude the position angle remains dominated by the primary mode. Above $9''$ up to 14° a

significant mode mixing is observed which corresponds to the trailing edge of the profile. The similarity of the polarization characteristics between the leading and the trailing components suggests that they might be arising from the same outer hollow cone of emission. The intense patch observed in the secondary mode between longitude $\sim -3''$ to -1° corresponds to the notch like feature in the profile, which is identified as the inner cone component. The polarization mode associated with the leading component goes over to this secondary component and a fair amount of mode mixing is observed as obvious from the faint tracks between $-5''$ to -3° . This probably suggests that the outer cone preferentially radiates in the primary mode and as one move inward to the inner cone, through a smooth mixing of the primary and the secondary mode, the secondary mode dominates in the inner cone. Similar character of the trailing part of the profile is also evident between 4° to $5''$ longitude, which corresponds to the fourth component in the profile (Kramer, 1995). It is evident that the outer and the inner conal rings exhibit polarization states which are approximately orthogonal to each other. The mode mixing tracks between the two cones are regions of transition from one cone to the other and the significant amount of depolarization observed along these tracks are probably due to the overlapping effects of the finite size of the cone, where the radiation from nearby field lines can direct radiation towards the line of sight. The central intense polarization mode lying between 0° to $2''$ corresponds to the core emission (refer chapter 1, also see Rankin 1990). The position angle associated with the core is connected to the the secondary mode through a smooth mode mixing as seen in the figure.

4.3.6 Polarization modes at 4.850 GHz

A sequence of 2267 pulses observed using the 100-m Effelsberg radio telescope was used to produce the grey-scale plots of the frequency of occurrence of the position angles as shown in figure (4.8). The bin resolution in figure (4.8) is 0.6 msec, which is to ensure sufficient number of points in a particular bin. The scarcity of sample points as evident in the figure indicates that the pulsar has depolarised considerably at high frequency (Xilouris et al, 1995). However, the overall characteristics of the position angle traverse

0329+54 lovell 4.850 GHz 2250 pulses $T_{res}=0.9904$ rns

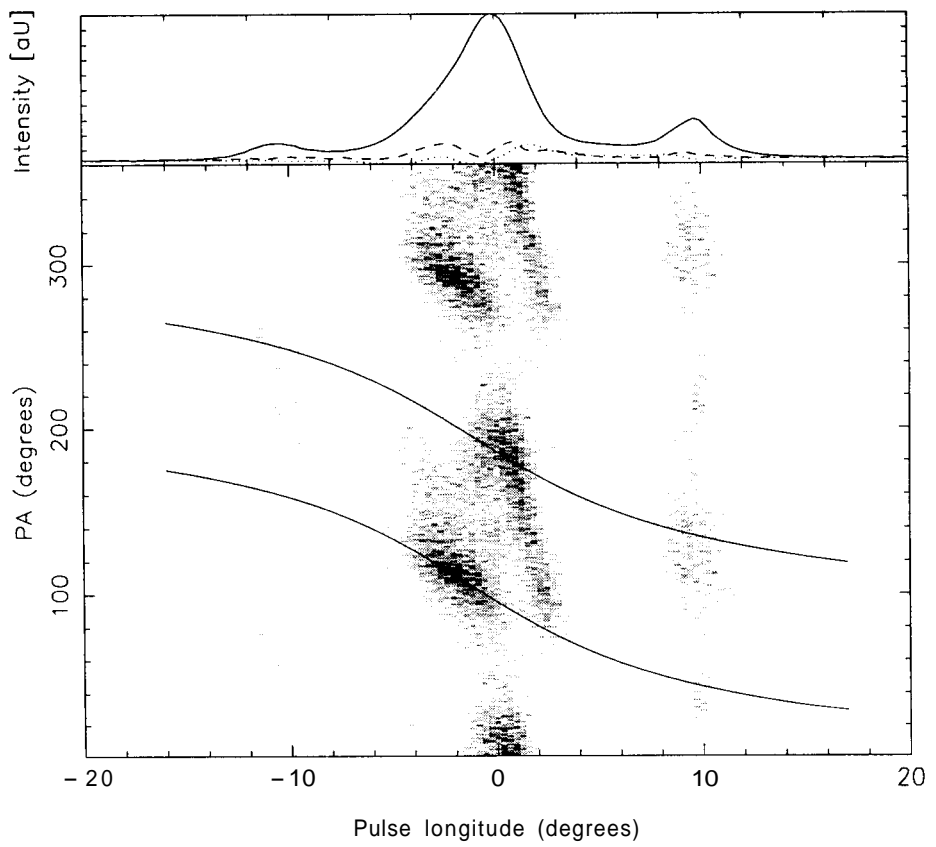


Figure 4.8: Grey scale representation of the position angle at 4.85 GHz. Refer section 4.3.6 for discussion.

are in good agreement with those observed at 2.695 GHz. Between -11° to -9° , there is a faint emission associated with the primary mode below the leading conal component. Between $-3''$ to -1° the secondary mode dominates. There is a sharp transition to the primary mode and a fair amount of non-orthogonal emission between 0° to $2''$. Finally at the trailing edge of the profile the position angle is dominated by the primary mode, but some weak presence of the secondary mode and some mode mixing is also observed between longitudes $\sim 8^\circ$ to 11° .

The dearth of sample points makes it difficult to fit the RVM to the observed position angle traverse. We have plotted the expected traverse using $a = 32.5^\circ$, $\beta = -3.5^\circ$, $\phi = -1.0$ and $\Psi_o = 105^\circ$, to illustrate the nature of the position angle traverse at lower frequencies. The intense patch observed in the secondary polarization mode gives the measured $(d\Psi/d\phi)_{\phi=\phi_o} \sim -10^\circ/^\circ$, which is consistent with that observed at lower frequencies. The sharp feature at 0° longitude is similar to the one which had developed at 2.695 GHz, but it extends for about $90''$ in the position angle and almost touches the secondary mode. $(d\Psi/d\phi)_{\phi=\phi_o} \sim -50^\circ/^\circ$ for this feature is quite consistent with that observed at 2.695 GHz.

4.4 Discussion

The multifrequency polarization position angle traverse of PSR B0329+54 show significant change over the frequency range 408 MHz to 4.8 GHz as discussed in the previous section. The RVM holds good for the outer edges of the profile over the whole frequency range, but the position angle traverse corresponding to the core component changes significantly. The overall effect across the profile, as clear from figure 4.7, can be interpreted as a change in impact parameter ($@$) as a function of frequency. A possible explanation for such an effect is the presence of multipolar magnetic fields in neutron stars as discussed in section 4.2.

Multipolar magnetic fields at the surface of the neutron star are invoked to explain the radio emission from pulsars (cf. chapter3). Further some theoretical models of the generation of magnetic fields of neutron stars predict non-dipolar field structures

(Urpin et al. 1986). However in the observational front there has been no clear evidence for the presence of multipolar magnetic fields. As a possibility we have shown that the deviations from the RVM, as discussed in section (4.1) can arise due to the presence of multipolar fields that are sufficiently strong in the emission region (Radhakrishnan 1990). As seen in figure (4.1), a mixture of dipole and quadrupole components can give rise to kinks in the polarization position angle curve near the profile center. Such kinky features are often observed in several core dominated pulsars (e.g. also in PSR B1237+25). The other point to be noted is that towards the wings of the simulated position angle curves the traverse is similar to that given by the RVM.

We model the emission of PSR B0329+54 above 2 GHz to be arising from regions where the underlying magnetic field is approximated by a dipole and at least a quadrupole. Emission below 2 GHz, appears to originate from regions with largely dipolar magnetic field geometry, while emission above 2GHz shows the evidence of departure from pure dipole configurations. The orientation of the quadrupole with respect to the dipole and the strength of the quadrupole are unknowns in this problem, which makes it difficult to seek an unique model. We varied the parameters $\theta_1, \theta_2, \theta_3$, which defines the orientation of the quadrupole with respect to the dipole and the ratio Q (refer section 4.1), to find trends that might explain the observed position angle traverse observed at 2.7 GHz (fig.4.7) and above. For $\theta_1 = 37^\circ, \theta_2 = 0^\circ, \theta_3 = 0^\circ$ $Q = 1$ and $r = 7$, the simulated position angle curve is in good agreement with the position angle traverse at 2.7 GHz as shown in figure (4.9). The values of a and β are chosen to be 32.5° and $-3''$ respectively.

One of the important assumptions made in putting forward the above explanation for the frequency dependence of the polarization position angle is the existence of a radius-to-frequency mapping in pulsars. The outer conal widths (defined as half power points of the outer cone) of PSR B0329+54 show a systematic decrease with increasing frequency (refer fig 4.10), but for frequencies above 2 GHz the widths appear to become nearly independent of frequency. Assuming a dipolar magnetic field geometry, the emission height at each frequency can be inferred from equation (1.18) of chapter 1. Assuming $a = 32.5''$ and $\beta = 3.0^\circ$, the emission heights for frequencies 102 MHz to 10

0329+54 effberg 2.695 GHz 2250 pulses $T_{res}=1.145$ ms

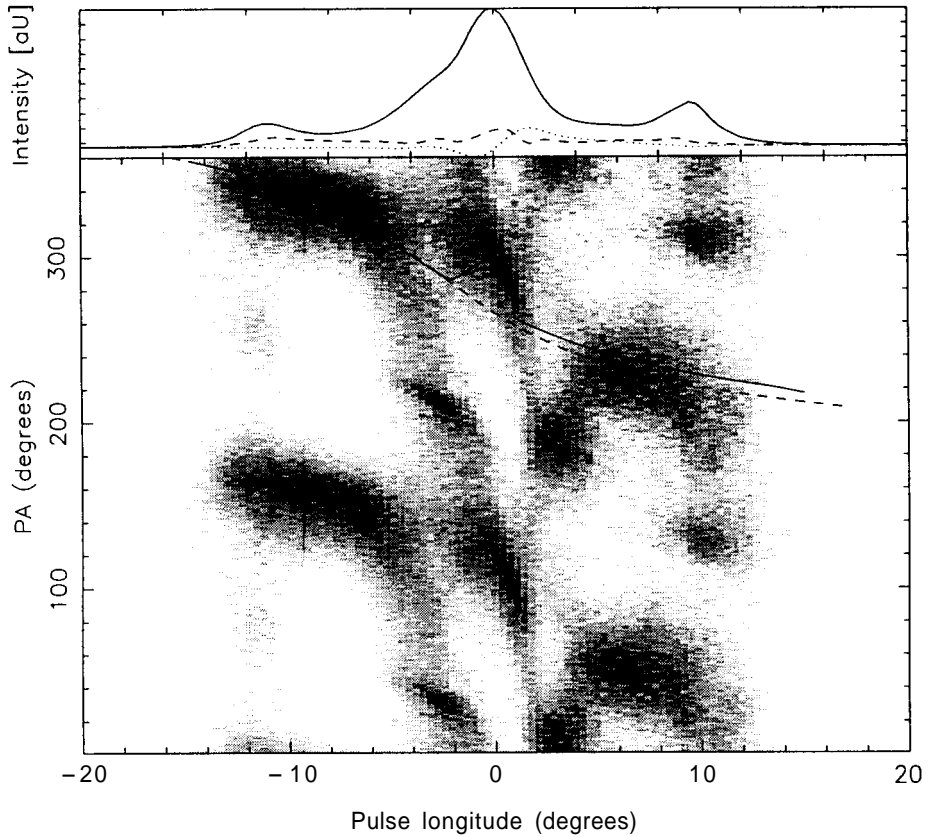


Figure 4.9: Same as figure 4.7. In the bottom panel, the continuous line is the model for the position angle curve for a multipolar field structure which is a mixture of a dipole and a quadrupole. The parameters for the curve are $Q = 1$, $\theta_1 = 37^\circ$, $\theta_2 = 0^\circ$, $\theta_3 = 0^\circ$ and the emission height as 7 times the stellar radius. a and β for the curve is assumed to be $32.5''$ and $-3''$ respectively. The dashed line corresponds to the RVM with $a = 32.5^\circ$, $\beta = -3^\circ$, $\Psi_o = 290^\circ$ and $\phi_o = -2.7''$ respectively.

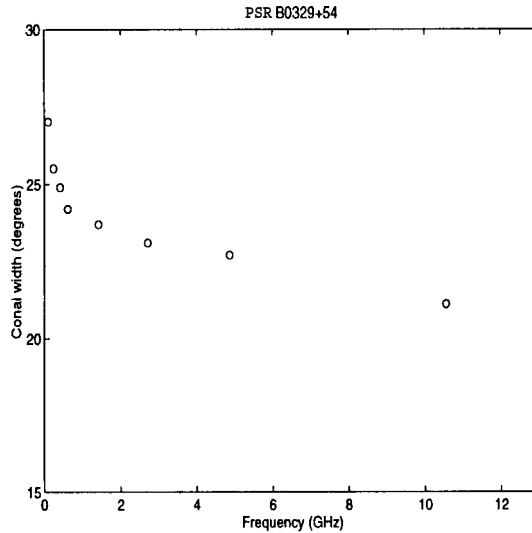


Figure 4.10: Conal widths versus frequency plot for PSR B0329+54. The above plot is made from the data provided to us by Rankin (1999).

GHz ranges from about 270 km to 180 km. Emission height constraints obtained from timing analysis (Kramer et al. 1997) also suggest that the radio emission arises from a narrow range of heights. Following curvature emission as the basic emission mechanism, the characteristic frequency of emission depends on the lorentz factor and the radius of curvature of the last open dipole field line κ as γ^3/κ . The radius of curvature over this emission region practically remains constant if a dipole field geometry is assumed. Thus γ has to change by a factor of five over this small range in order to explain the broad band emission. This does not appear to be possible within the framework of any theoretical model (e.g. Ruderman & Sutherland 1975, Beskin et al. 1988, 1993). An alternative explanation would be to introduce a rapid change of radius of curvature through the emission region, as would be expected in the presence of higher multipole components of the magnetic field. Of course, in such a picture, emission heights themselves would have to be re-determined self-consistently.

The core emission, below which the polarization position angle curve has developed kinkiness, also exhibits significant circular polarization signatures (refer Fig. 4.3). This signature, which is typical for cores in pulsars, might arise if the emission is due to particles with small ($\sim 10-20$) lorentz factors (Radhakrishnan & Rankin 1990). The

antisymmetric nature of the circular polarization (as clearly visible in the 2.7 GHz profile in Fig 4.3) is expected from curvature radiation as seen in figure 1.7. In case such low γ particles are present then the observer's line-of-sight, while crossing the core, will simultaneously receive radiation from particles moving in several nearby field lines. In the case of dipolar geometry of the magnetic field, the particles moving in the adjacent field lines will be seen to move in curved trajectories, and the radiation observed will be in general elliptically polarized. The observer thus receives a mixture of linear and circular polarizations at a given point. Incoherent addition of radiations from different field lines will lead to effective depolarization, and will cause a 'smoothing' of the polarization position angle curve. Such depolarization is observed in pulsars with increasing frequency (Xilouris et al. 1995) and is also clearly seen in our analysis: the linearly polarized power, strong at low frequencies, has decreased considerably at 4.8 GHz (figure 4.8). However it is unlikely that emission from low γ particles can cause kinkiness in the polarization position angle curve which is only seen at higher frequencies (~ 2.7 GHz and above).

Aberration effects can further cause changes in the position angle traverse, as mentioned in section (4.1). Detailed investigation by Blaskewicz et al. (1991) shows that the net effect of aberration is to delay the position angle curve with respect to the pulse profile. The shape of the polarization position angle traverse, however, does not change. Moreover, aberration effects are only important when the corotation velocities are high. For emission arising near the stellar surface such effects are negligible. There can also be a displacement of the emission region in the azimuthal direction (Kapoor & Shukre, 1998), which can cause the effective β to change with frequency. but again the effects will be prominent only at much higher altitudes while the estimated emission heights for PSR B0329+54 are rather small.

We have shown that a dipolar magnetic field structure is not sufficient to explain the multifrequency linear polarization characteristics of PSR B0329+54. Instead a mixture of dipole and quadrupole can possibly explain the spectral variations of the polarization position angle. The characteristic age of PSR B0329+54 is estimated to be 5.5 Myr, making it a relatively old pulsar. If the observed structure is indeed due

to the presence of multipole components of the magnetic field, then this reinforces the conclusion of chapter 3 about the long-term stability of the multipole structure. In conclusion we suggest that the polarization signature observed in PSR. B0329+54 may be an indicator to the presence of magnetic niultipoles in this pulsar. Similar investigations are required for other pulsars to get a clear picture of the magnetic field structiire.